Journal of Neurochemistry

JOURNAL OF NEUROCHEMISTRY | 2016 | 139 | 610–623 doi: 10.1111/jnc.13763

ORIGINAL ARTICLE

Tyrosine kinase inhibition reverses TDP-43 effects on synaptic protein expression, astrocytic function and amino acid dis-homeostasis

Lanier Heyburn,*·† Michaeline L. Hebron,* Jacqueline Smith,‡ Charisse Winston,§ John Bechara,* Zhaoxia Li,*·¶ Irina Lonskaya,* Mark P. Burns,§ Brent T. Harris*·† and Charbel E.-H. Moussa*

*Laboratory for Dementia and Parkinsonism, Department of Neurology, Georgetown University Medical Center, Washington, District of Columbia, USA

†Department of Pathology, Georgetown University Medical Center, Washington, District of Columbia, USA

‡Drug Discovery Center, Georgetown University Medical Center, Washington, District of Columbia, USA

§Trauma and Dementia Laboratory, Department of Neuroscience, Georgetown University Medical Center, Washington, District of Columbia, USA

¶School of Traditional Chinese Medicine, Capital Medical University, Fengtai District, Beijing, China

Abstract

The trans-activating response of DNA/RNA-binding protein (TDP)-43 pathology is associated with many neurodegenerative diseases via unknown mechanisms. Here, we use a transgenic mouse model over-expressing human wild-type neuronal TDP-43 to study the effects of TDP-43 pathology on glutamate metabolism and synaptic function. We found that neuronal TDP-43 over-expression affects synaptic protein expression, including Synapsin I, and alters surrounding astrocytic function. TDP-43 over-expression is associated with an increase in glutamate and γ-amino butyric acid and reduction of glutamine and aspartate levels, indicating impairment of presynaptic terminal. TDP-43 also decreases tricarboxylic acid cycle metabolism and induces oxidative stress via lactate accumulation. Neuronal TDP-43 does not alter microglia activity or significantly changes systemic and brain inflammatory markers compared to control. We previously demonstrated that brain-penetrant tyrosine kinase inhibitors (TKIs), nilotinib and bosutinib, reduce TDP-43-induced cell death in transgenic mice. Here, we show that TKIs reverse the effects of TDP-43 on synaptic proteins, increase astrocytic function and restore glutamate and neurotransmitter balance in TDP-43 mice. Nilotinib, but not bosutinib, reverses mitochondrial impairment and oxidative metabolism. Taken together, these data suggest that TKIs can attenuate TDP-43 toxicity and improve synaptic and astrocytic function, independent of microglial or other inflammatory effects. In conclusion, our data demonstrate novel mechanisms of the effects of neuronal TDP-43 over-expression on synaptic protein expression and alteration of astrocytic function.

Keywords: astrocytes, TDP-43, tyrosine kinase inhibition.

J. Neurochem. (2016) **139**, 610–623.

Received June 3, 2016; revised manuscript received July 22, 2016; accepted August 2, 2016.

Address correspondence and reprint requests to Charbel E.-H. Moussa, MD, PhD, Laboratory for Dementia and Parkinsonism, Translational Neurotherapeutics Program, Department of Neurology, Georgetown University School of Medicine, 4000 Reservoir Rd, NW, Building D, Room 203-C, Washington, DC 20057, USA. E-mail: cem46@georgetown.edu

Abbreviations used: ALS, amyotrophic lateral sclerosis; Asp, aspartate; C-C, chemokines; Cit, citrate; DMSO, dimethyl sulfoxide; EAAT, excitatory amino acid transporters; FTLD-TDP, frontotemporal lobar degeneration with TDP-43; GABA, γ-amino butyric acid; GFAP, glial fibrillary acidic protein; Gln, glutamine; Glu, glutamate; IBA-1, ionized calcium-binding adaptor molecule 1; IL, interleukin; Lac, lactate; Succ, succinate; TCA, tricarboxylic acid; TDP-43, TAR DNA-binding protein 43; TKI, tyrosine kinase inhibitor; TNF-α, tumor necrosis factor; VEGF, vascular endothelial growth factor.

The trans-activating response region of DNA-binding protein known as TDP-43 is a 414 amino acid polypeptide involved in regulation of the expression of thousands of genes via DNA/RNA binding and alternative splicing of pre-mRNAs (Polymenidou *et al.* 2011). Neurons in the spectrum of disorders of motor neuron disease and frontotemporal lobar degeneration (FTLD-TDP) are marked by ubiquitin-positive inclusions that mainly consist of TDP-43 (Neumann *et al.* 2006). The precise pathological role of TDP-43 remains unclear (Neumann *et al.* 2006). Previously, our group demonstrated that lentiviral over-expression of human TDP-43 leads to failure of amino acid homeostasis, including decreased conversion of glutamate to glutamine (Hebron *et al.* 2014). Thus, glutamate metabolism is an important area of research for TDP-43 pathologies.

Glutamate homeostasis is important for the maintenance of functional synapses (Zeng *et al.* 2007). There is currently ample evidence that TDP-43 plays an important role in synaptic function. TDP-43 regulates RNA processing of many genes that encode synaptic proteins, including presynaptic markers, synaptotagmin and glutamate transporters and receptors (Polymenidou *et al.* 2011; Honda *et al.* 2014). Local translation of proteins at the synapse is an important aspect of neuronal function. Control of this translation involves silencing of translation by mRNA silencing foci such as stress granules (Pascual *et al.* 2012). TDP-43 has been found in these stress granules, indicating that it may be involved in control of local synaptic translation. TDP-43 also plays a role in mRNA transport and local translation in dendritic spines (Wang *et al.* 2008; Sephton and Yu 2015). In response to neuronal stimulation, there is increased co-localization of TDP-43 with the dendritic spine marker postsynaptic density-95 protein (Wang *et al.* 2008), indicating that TDP-43 is activity responsive in postsynaptic neurons. Studies using *Drosophila* neuromuscular junctions revealed that TDP-43 is necessary for synaptic growth, formation and pruning (Godena *et al.* 2011; Lin *et al.* 2011). Therefore, the presence of TDP-43 at the synapse is likely important for the regulation of local protein translation and maintenance of normal synapses. Alterations in TDP-43 function as a result of mutation or mis-localization, as found in amyotrophic lateral sclerosis (ALS) and FTLD-TDP, may lead to deregulation of local synaptic translation and loss of synaptic maintenance.

Glutamate homeostasis and metabolic support of neurons are two important functions of astrocytes (Danbolt 2001). Astrocyte dysfunction can disrupt their ability to support neurons, leading to motor and non-motor neuron cell death (Philips and Rothstein 2014). Microglia are also involved in central nervous system (CNS) immunity and release pro-inflammatory and anti-inflammatory cytokines and chemokines in response to an insult and other cellular signals (Philips and Rothstein 2014). The various insults such as neuroinflammation and loss of glutamate homeostasis may contribute to neurodegeneration. Previous work with TDP-43 mouse models expressing mutant TDP-43^{A315T} or TDP-43^{M337V} shows increased reactive astrogliosis and microglial activation (Wegorzewska *et al.* 2009; Stallings *et al.* 2010). This gliosis has also been observed in mouse models over-expressing human wild-type TDP-43 (Xu *et al.* 2010). Taken together, these findings suggest that cellular inflammation is another important aspect of TDP-43 pathology. Understanding how TDP-43 pathology contributes to neuroinflammation and astrocytic function is important for understanding disease pathogenesis and for the identification of therapeutic targets.

We previously demonstrated that some brain-penetrant tyrosine kinase inhibitors (TKIs) may be a potential alternative strategy to ameliorate the pathology associated with protein aggregation in neurodegenerative diseases (Hebron *et al.* 2013; Lonskaya *et al.* 2013a, 2014). We previously demonstrated that at 4 h plasma : brain nilotinib (10 mg/kg) and bosutinib (5 mg/kg) peaks at 3% and 5%, respectively, and they both inhibit brain tyrosine kinase Abelson (Abl) activity (Hebron *et al.* 2013; Lonskaya *et al.* 2013a, 2014). Nilotinib and bosutinib are clinically effective and well-tolerated FDA-approved treatments for chronic myeloid leukemia (Kantarjian *et al.* 2007; Musumeci *et al.* 2012). We have shown that nilotinib and bosutinib reverse motor and cognitive decline and reduce TDP-43-induced cell death in the cortex and spinal cord of transgenic mice that over-express human wild-type TDP-43 (Chen *et al.* 2014). In this study, we used a hemizygous transgenic mouse that over-expresses human wild-type TDP-43 in neurons (Wils *et al.* 2010) and investigated how neuronal TDP-43 pathology affects glutamate homeostasis, synaptic maintenance and the immune profile. We treated these mice with TKIs to further investigate tyrosine kinase inhibition as potential new therapeutic tools for TDP-43 pathologies.

Materials and methods

Mice and treatment

Six-month-old male and female hemizygous mice that express human wild-type TDP-43 under the control of the neuron-specific Thy-1 promoter (Wils *et al.* 2010) obtained from Jackson laboratories (n = 16) and non-transgenic littermates (n = 16) were treated with intraperitoneal (I.P.) injection (30 μL) of either 10 mg/kg nilotinib, 5 mg/kg bosutinib or dimethyl sulfoxide (DMSO) every day for 4 weeks. A total of 36 transgenic animals and 36 non-transgenic control littermates were used in this study. Nilotinib (Cat# S1033) and bosutinib (Cat# S1014) were commercially obtained (Selleckchem Inc., Houston, Texas, USA) in 10 mg vials and dissolved in 1 mL DMSO (50 mg/mL), aliquoted to avoid freeze and thaw cycles and stored at −20°C. A total volume of 30 μL solution with a final concentration of 10 mg/kg nilotinib or 5 mg/kg bosutinib was injected. All animal experiments were conducted in full compliance with the recommendations of Georgetown University Animal Care and Use Committee (GUACUC).

Grip strength test

Animals were placed on a wire rack that was then inverted. Latency to fall was recorded as the time (in seconds) it took for the animal to fall from the wire rack. These mice were also weighed biweekly. $N = 3$ for controls, $N = 22$ for transgenic mice ($N = 7$ DMSO, $N = 8$ nilotinib, $N = 7$ bosutinib).

Open field test

Animals were placed in individual, empty boxes and allowed to explore for 1 h. Overhead cameras captured the animals' movements. Movement was analyzed using ANY-maze software (Stoeling Co, Wood Dale, IL, USA). Total distance traveled (in meters) and time spent in the center zone (in seconds) were recorded and used for analysis. Time in center divided by total distance traveled was calculated. One-way ANOVA was performed. $N = 3$ for controls, $N = 22$ for transgenic mice ($N = 7$ DMSO, $N = 8$ nilotinib, $N = 7$ bosutinib).

Milliplex enzyme-linked immunosorbent assay

Animals were deeply anesthetized with a mixture of xylazine and ketamine (1 : 8) and 50–150 μL of whole blood was collected via cardiac puncture, centrifuged at 15 000 *g* to precipitate blood cells and the supernatant was examined by enzyme-linked immunosorbent assay (ELISA). To wash out the remaining blood from vessels and reduce contamination, animals were perfused with 10 mL of 1× saline for 4 min and the brain was collected and immediately homogenized in 0.5 mL ELISA buffer. We customized a highly sensitive and unbiased Milliplex® MAP Kit (Cat # MPXMCYTO-70K; Millipore Corporation, Bedford, MA, USA) with color-coded microspheres and fluorescent dyes, which through precise concentrations, the beads can simultaneously and specifically capture mouse immune molecules including interleukin (IL)-1α, IL-1β, IL-2, IL-4, IL-6, IL-10, IL-13, IFN-γ, TNFα, CCL2, CCL5 and vascular endothelial growth factor (VEGF). A total of 25 μL of sample was introduced into a plate containing the microspheres and the reaction mixture was incubated with Streptividin-PE conjugate and the reporter molecule as described in the manufacturer's protocol. Using a Luminex® machine, microspheres are first passed through a laser which excites the internal dyes making the microspheres; and a second laser that excites the PE, which is the fluorescent dye on the reporter molecule, and then a high-speed digital signal processor identifies each individual microsphere and quantifies the bioassay in terms of mean fluorescent intensity. $N = 4$ for each treatment group.

Immunohistochemistry of brain sections

Animals were deeply anesthetized with a mixture of xylazine and ketamine (1 : 8), washed with 1× saline for 1 min and then perfused with 4% paraformaldehyde for 15–20 min. Brains were quickly dissected out and immediately stored in 4% paraformaldehyde for 24 h at 4°C, and then transferred to 30% sucrose at 4°C for 48 h. Brains were cut using a cryostat at 4°C into 20-micron-thick coronal sections and stored at −20°C. Mouse and human TDP-43 was probed (1 : 200) with rabbit polyclonal (ALS10) antibody (cat# 10782-2-AP; ProteinTech, Chicago, IL, USA). Glial fibrillary acidic protein (GFAP) was probed (1 : 200) with mouse anti-GFAP (ms-1376-P; ThermoScientific, Rockville, MD, USA). Synaptotagmin was probed (1 : 200) with mouse monoclonal anti-synaptotagmin-12 (820401; BioLegend, San Diego, CA, USA). Synapsin I was probed (1 : 200) with rabbit polyclonal anti-synapsin I (GTX82594; GeneTex, Irvine, CA, USA). Iba-1 was probed (1 : 200) with rabbit anti-Iba1 (019-19741; Wako, Richmond, VA, USA). 4',6-diamidino-2-phenylindole (DAPI) staining was performed according to manufacturer's instructions (Sigma, St Louis, MO, USA). All staining experiments were scored by an investigator blinded to the treatments. $N = 4$ for each treatment group.

Golgi staining, microscopic analysis and Sholl analysis

For detailed characterization of neuronal processes and spines, Golgi staining was performed using the FD Rapid Golgi Stain Kit (FD NeuroTechnologies, Ellicott City, MD, USA), as reported previously (Winston *et al.* 2013). Briefly, after sacrifice, brains were removed from the mice and immersed in solutions A and B for 2 weeks at 25°C and then transferred into solution C for 48 h at 4°C. The brains were sliced using a Vibratome (WT1000S; Leica, Weztler, Germany) at a thickness of 150 μm. Bright-field microscopy images of pyramidal neurons in layers II/III of the cortex and granule neurons in the dentate gyrus of the hippocampus were captured using 63× oil immersion objective on a Zeiss Axioplan 2 (Brighton, MI, USA). The numbers of dendritic spines on apical oblique (AO) and basal shaft (BS) dendrites were quantified in the analysis. AO dendrites project off the apical dendrite, and counts only incorporated a 20-μm section of the primary AO. BS dendrites project directly off the cell soma, and counts incorporated dendritic spines along a 20-μm section of the shaft between 30 and 100 μm away from the soma. Different neurons were used to quantify AO and BS segments of healthy pyramidal neurons of cortical layers II/III. Images were coded, and dendritic spines were counted in a blinded fashion using Image J Software (National Institutes of Health, Bethesda, MD, USA). $N = 4$ for each treatment group.

For Sholl analysis, images of the Golgi-stained pyramidal neurons were overlaid with concentric circles, consisting of a 10-μm radius between each circle. The concentric circles spanned from 0 to 70 μm, with a radial interval of 10 μm between each circle. The center point of the circles was superimposed over the cell body of previously acquired Golgi-stained neurons, and the number of apical and basal shaft dendrites crossing each circle was manually counted and plotted as number of crossings against distance from soma.

Stereological methods

Stereological methods were applied by a blinded investigator using unbiased stereology analysis (Stereologer; Systems Planning and Analysis, Chester, MD, USA) to determine the total positive cell counts in 20 cortical fields on at least 10 brain sections (~ 400 positive cells per animal) from each animal as previously explained (Algarzae *et al.* 2012). Cortical synaptotagmin-positive staining was assessed by optical density (OD) measurements. Using an Optronics (Goleta, CA, USA) digital camera and a constant illumination table, digitalized images of synaptotagmin immunostained cortical sections were collected. ODs were measured using Image-Pro Plus software (Version 3.0.1; Media Cybernetics, Silver Spring, MD, USA). The OD was measured from six cortical coronal sections and the final reading was calculated as an average of those values. Nonspecific background correction in each section was done by subtracting the OD value of the corpus callosum from the cortical OD value obtained from the same section. The OD analysis was performed under blinded condition.

High-frequency $^{13}C/^{1}H$ nuclear magnetic resonance spectroscopy

Animals were fasted overnight with free access to tap water and were I.P. injected with [1-^{13}C] glucose solution (0.5 mol/L) over 10 s (0.3 mL/25–30 g body weight; 200 mg/kg). Forty-five minutes later, animals were killed by cervical dislocation and hemispheres were isolated and immediately homogenized in 6% ice-cold perchloric acid, 50 mM NaH_2PO_4. After homogenization, the perchloric acid de-proteinized supernatant was separated by centrifugation at 14 000 *g* for 30 min, frozen on dry ice and lyophilized overnight. Extracts were then re-suspended in 0.65 mL D_2O containing 2 mM sodium [^{13}C] formate as internal intensity and chemical shift reference (δ 171.8). Metabolite pool size was identified on ^{1}H {^{13}C-decoupled} nuclear magnetic resonance (NMR) spectra. Peak areas were adjusted for nuclear Overhauser effect, saturation and natural abundance effects and quantified by reference to [^{13}C] formate. Metabolize pool sizes were determined by integration of resonances in 400 MHz {^{13}C-decoupled} ^{1}H spetra using *N*-acetylaspartate as internal intensity reference. Incorporation of ^{13}C isotopomers was measured in reference to [^{13}C] formate. ^{13}C [^{1}H-decoupled] spectra typically 30 000–33 000 transients, pulse width is 4 s, 83 000 data points were acquired at 9.7 Tesla Varian Spectrometer (Varian, Santa Clara, CA USA) with dual $^{13}C/^{1}H$ probe. {^{13}C-decoupled}-^{1}H spectra were acquired with 3000 scans, pulse angle 45°, relaxation delay 1 s, line broadening 0.5 Hz, acquired data points 13.132 and transformation size 32K at 25°C. Spectra were integrated and quantified using MestReNova (Master Lab Research, Escondido, CA). $N = 4$ for each treatment group.

Cell culture, transfection and RT-PCR

Human neuroblastoma SH-SY5Y cells were grown in 24-well dishes (Falcon, Bedford, MA, USA) as described previously (Rebeck *et al.* 2010; Lonskaya *et al.* 2013b). Transient transfection was performed with 3 μg TDP-43 cDNA or 3 μg LacZ cDNA for 12 h. Cells were treated with 10 μM nilotinib or 5 μM bosutinib for an additional 12 h and harvested 48 h after transfection. qRT-PCR was performed on real-time Polymerase chain reaction (PCR) system (Applied Biosystems, Foster City, CA, USA) with Fast SYBR-Green PCR master Mix (Applied Biosystems) in triplicate from reverse-transcribed cDNA from human neuroblastoma SH-SY5Y cells transfected with LacZ or TDP-43 treated with DMSO, nilotinib or bosutinib and gene expression values were normalized using GADPH levels.

Western blot analysis

The cortex was dissected out or human neuroblastoma SH-SY-5Y cells were homogenized in 1× STEN buffer then centrifuged at 5000 *g* and the supernatant was collected as indicated previously (Rebeck *et al.* 2010; Lonskaya *et al.* 2013b). Total TDP-43 was probed with (1 : 1000) rabbit polyclonal (ALS10) antibody (10782-2-AP; ProteinTech), Synapsin I was probed (1 : 1000) with rabbit polyclonal anti-Synapsin I (GTX82594; GeneTex) and actin was probed (1 : 1000) with rabbit polyclonal anti-actin (Thermo Scientific). Glutamate transporters were probed with rabbit polyclonal anti-excitatory amino acid transporter-1 (1 : 1000) antibody (Cell Signaling Technology, Beverly, MA, USA), and rabbit polyclonal anti-EAAT2 (1 : 1000) antibody (Cell Signaling Technology). Western blots were quantified by densitometry using Quantity One 4.6.3 software (Bio-Rad Laboratories, Hercules, CA, USA). Densitometry was obtained as arbitrary numbers measuring band intensity. Data were analyzed as mean ± SEM, using ANOVA with Neumann–Keuls multiple comparison between treatments.

Statistical analysis

Data were analyzed using GraphPad PRISM software (San Diego, CA) and statistical analysis was performed using one-way ANOVA, Neumann–Keuls, $p < 0.05$ or as indicated, n is indicated in the text, and graphs were plotted mean ± SEM.

Results

Mouse characterization

We first characterized our mouse model using various measurements. The homozygous over-expressers (TDP-43$^{+/+}$) published by Wils *et al.* (2010) exhibit signs of muscle weakness and inflammation. When breeding, our homozygous over-expressers became weak, paralyzed and hunched (Figure S1a) at around postnatal day 7 (P7) and died before weaning. This phenotype in homozygous TDP-43$^{+/+}$ mice is reminiscent of an ALS-like pathology. Therefore, we decided to use the hemizygous mouse line as these mice live much longer but still have TDP-43 over-expression. To investigate the effects of neuronal TDP-43 on the phenotype we used aged TDP-43 transgenic mice (1- and 2-year-old). We performed a grip strength test to determine whether the mice exhibit any muscle weakness. We found that the oldest mice show a slightly decreased latency to fall compared to the 1-year-old mice (Figure S1b). Weights were also measured to determine whether there was any wasting away of these mice and we found no significant difference in weights between controls, 1-year-old and 2-year-old transgenic mice (Figure S1c). We then performed an open field test in order to measure locomotion and anxiety. TDP-43 mice traveled significantly more than non-transgenic littermates (Figure S1d), suggesting hyperactivity. The transgenic mice also spent less time in the center zone compared to non-transgenic mice, though this was not significant (Figure S1e). Transgenic mice spent significantly less time in the center zone relative to distance travelled compared to non-transgenic littermates. When mice were treated with daily I.P. injection (30 μL) of either 10 mg/kg nilotinib, 5 mg/kg bosutinib or DMSO for 4 weeks, bosutinib but not nilotinib reversed the time spent in the center zone toward control level (Figure S1f). TKIs had no effect on weight or grip strength in these mice (data not shown).

TKIs ameliorate loss of amino acid homeostasis in TDP-43 transgenic mice

High-frequency $^{13}C/^{1}H$ NMR spectroscopy was performed in cortical extracts to compare the effects of neuronal TDP-43 over-expression on conversion of glutamate into glutamine by astrocytes. ^{13}C MRS shows that TDP-43 transgenic mice had a significantly increased concentration of ^{13}C-labeled

glutamate (Glu) C4 compared to non-transgenic controls (Fig. 1a, $n = 4$). Daily treatment with either nilotinib or bosutinib for 4 weeks reversed ^{13}C concentration to non-transgenic levels (Fig. 1a, $n = 4$). Neuronal TDP-43 over-expression decreased ^{13}C-labeled glutamine (Gln) C4 compared to non-transgenic levels (Fig. 1a, $n = 4$), and nilotinib and bosutinib reversed the decrease in ^{13}C-labeled glutamine (Fig 1a, $n = 4$). TKIs had no effects on glutamate levels in non-transgenic control mice (data not shown). ^{1}H MRS also shows that TDP-43 transgenic mice had significantly higher levels of total glutamate and a decrease in total glutamine, which were significantly reversed by treatment with either nilotinib or bosutinib (Fig. 1b, $n = 4$). Aspartate is an excitatory amino acid that can be transported by excitatory amino acid transporters (EAATs) similar to glutamate. In neurons, pyruvate is predominantly converted to C2 aspartate via pyruvate dehydrogenase, while in glia, it is converted to both C2 and C3 aspartate by pyruvate carboxylase. Examining concentrations of aspartate C2 and C3 can give insight into neuronal versus glial activity. TDP-43 transgenic mice had significantly decreased ^{13}C concentrations of both aspartate C2 and C3 compared to non-transgenic mice (Fig. 1c, $n = 4$). This decrease was ameliorated by treatment with nilotinib and bosutinib (Fig. 1c, $n = 4$). Importantly, there was a significantly lower concentration of predominantly glial-derived aspartate C3 compared to C2 (Fig. 1c, $n = 4$), indicating that astrocytic function may be impaired in the transgenic mice. TDP-43 transgenic mice also have significantly less total aspartate than non-transgenic mice, an effect that is reversed by tyrosine kinase inhibitor (TKI) treatment (Fig. 1d, $n = 4$). No differences in measured amino acids were observed with DMSO or TKIs in non-transgenic controls (data not shown).

Because we detected impairment in the neuron-astrocyte glutamate–glutamine cycle and an increase in glutamate levels, we further examined the fate of glutamate. Inhibitory neurons convert glutamate into the inhibitory neurotransmitter γ-aminobutyric acid (GABA). ^{13}C MRS shows that TDP-43 transgenic mice have significantly higher concentrations of ^{13}C-labeled GABA than non-transgenic mice, and that

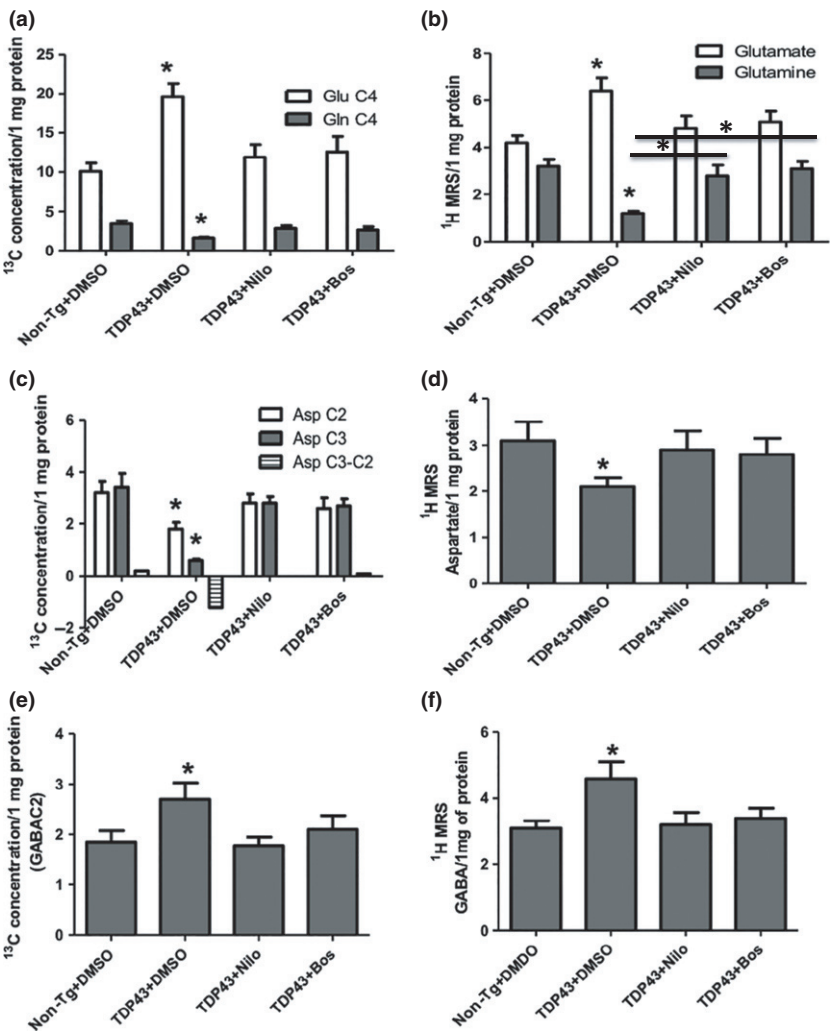

Fig. 1 High-frequency ^{13}C nuclear magnetic resonance spectroscopy reveals alteration in the levels of amino acids and γ-amino butyric acid (GABA). Histograms represent (a) ^{13}C concentration derived from glucose in Glu C4 and Gln C4 and (b) pool size of total glutamate and glutamine in brains of non-transgenic as well as transgenic mice treated with dimethyl sulfoxide (DMSO) (control), nilotinib or bosutinib. (c) ^{13}C concentration in Asp C2 and C3 and (d) pool size of aspartate in brains of non-transgenic as well as transgenic mice treated with DMSO, nilotinib or bosutinib. (e) ^{13}C concentration of GABA C2 and (f) pool size of total GABA in non-transgenic and transgenic mice treated with DMSO, nilotinib or bosutinib. Asterisk indicates significantly different from non-transgenic, mean ± SEM, two-way ANOVA, Neumann–Keuls, $n = 4$. $p < 0.05$.

TKIs reverse this increase (Fig. 1e, $n = 4$). Total levels of GABA are increased in TDP-43 transgenic mice and nilotinib and bosutinib bring these levels back to non-transgenic levels (Fig. 1f, $n = 4$).

TKI treatment aids in synaptic maintenance in TDP-43 transgenic mice

Astrocytes and the glutamate–glutamine cycle are critical for the maintenance and function of the synapse. In order to investigate how over-expression of TDP-43 in neurons affects the synapse, immunohistochemistry (IHC) was performed on cortical brain sections in order to visualize levels of TDP-43 and the presynaptic marker synaptotagmin-12. TDP-43 transgenic mice (Fig. 2b and e, $n = 4$) showed an increase in TDP-43 levels compared to non-transgenic littermates (Fig. 2a and e $n = 4$) as we demonstrated previously (Chen *et al.* 2014). Stereological counting shows that synaptotagmin-12 expression is greatly reduced in the transgenic mice (Fig. 2b and f, $n = 4$) compared to non-transgenic controls (Fig. 2a and f, $n = 4$), suggesting loss of presynaptic maintenance. We previously demonstrated that nilotinib and bosutinib decrease TDP-43 levels in transgenic mice over-expressing human TDP-43 via autophagy and protect against cell death (Chen *et al.* 2014). Treatment with nilotinib or bosutinib decreases expression of TDP-43 and restores expression of synaptotagmin-12 (Fig. 2c–f, $n = 4$), suggesting that TKIs decrease over-expression of TDP-43 as we demonstrated previously (Chen *et al.* 2014), therefore contributing to presynaptic maintenance. DMSO and TKIs did not affect endogenous TDP-43 (Chen *et al.* 2014) and

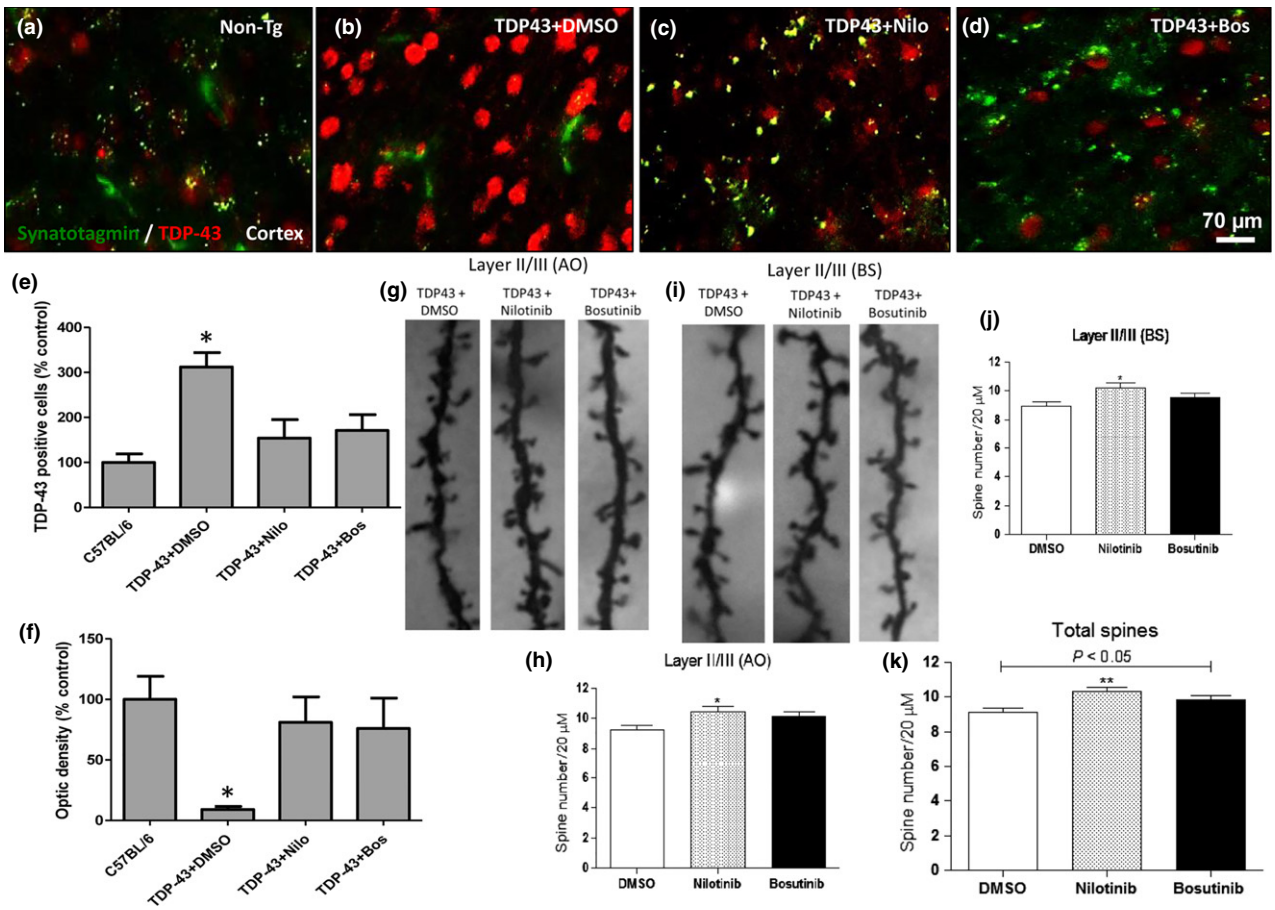

Fig. 2 Immunohistochemistry and Golgi stains reveal changes in synaptic maintenance in TAR DNA-binding protein 43 (TDP-43) transgenic mice. TDP-43 and synaptotagmin-12 staining of 20-μm-thick cortical sections from (a) non-transgenic (Non-Tg) as well as TDP-43 transgenic mice treated with (b) dimethyl sulfoxide (DMSO) (control), (c) nilotinib or (d) bosutinib. (e) Number of TDP-43-positive cells as a percent of control levels, as determined by stereological methods. (f) Optic density of synaptotagmin-12 staining, as a percent of control levels. (g) Silver stain of apical oblique dendrites and (h) quantification of the number of dendritic spines on the apical oblique per 20 μm in TDP-43 transgenic mice treated with DMSO, nilotinib or bosutinib. (i) Silver stain of basal shaft dendrites and (j) quantification of the number of dendritic spines on the basal shaft per 20 μm in TDP-43 transgenic mice treated with DMSO, nilotinib or bosutinib. (k) Total number of dendritic spines per 20 μm in TDP-43 transgenic mice treated with DMSO, nilotinib or bosutinib. Asterisk indicates significantly different from non-transgenic, mean ± SEM, ANOVA, Neumann–Keuls, $n = 4$. *$p < 0.05$, **$p < 0.01$.

synaptotagmin-12 levels in non-transgenic control mice (data not shown). Golgi staining was performed in order to visualize dendritic spines, sites of excitatory synapses. Compared to non-transgenic mice, TDP-43 transgenic mice treated with DMSO do not have a significant change in spine count (data not shown). However, TDP-43 transgenic mice treated with nilotinib have a significant increase in the number of dendritic spines in both the basal shaft and apical oblique dendrites (Fig. 2g–j, $n = 4$). TDP-43 transgenic mice treated with bosutinib show a trend to have more dendritic spines in the basal shaft and apical oblique dendrites, but this is not significant (Fig. 2g–j, $n = 4$). When analyzing the total number of dendritic spines, both nilotinib and bosutinib significantly increased the total number of dendritic spines compared to DMSO-treated TDP-43 mice (Fig. 2k, $n = 4$). The increase in total number of spines after treatment with TKIs indicates an increase in synapses in these mice.

To ascertain the effects of TDP-43 accumulation on synaptic maintenance, we performed IHC for another presynaptic marker, Synapsin I. IHC showed decreased Synapsin I staining in the TDP-43 transgenic mice (Fig. 3b, $n = 3$) compared to non-transgenic littermates (Fig. 3a, $n = 3$). Treatment with either nilotinib (Fig. 3c, $n = 3$) or bosutinib (Fig. 3d, $n = 3$) increased levels of synapsin in the cortex. Using optic density of Synapsin I as a percentage of

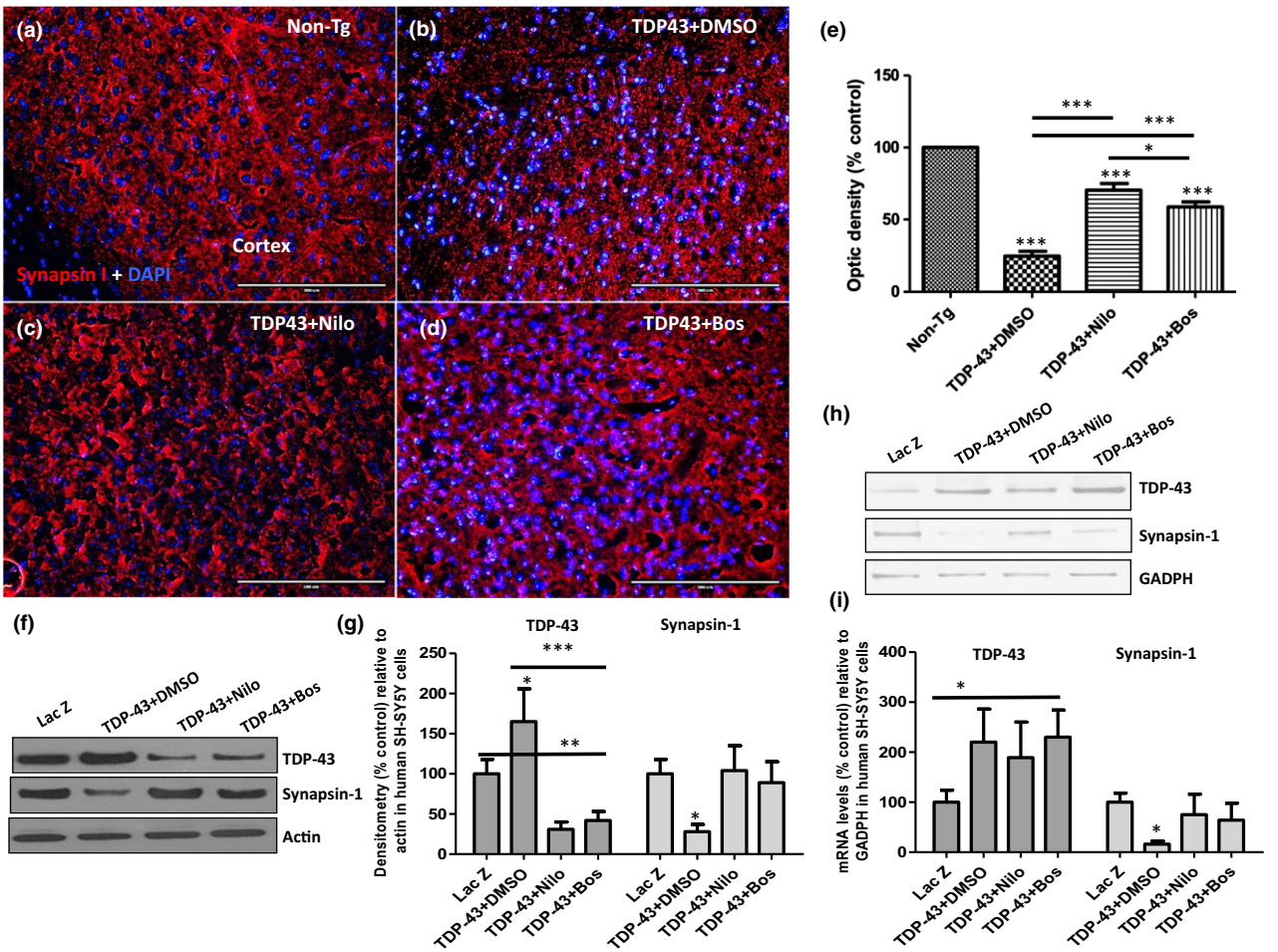

Fig. 3 Immunohistochemistry of mouse cortex shows changes in Synapsin I expression in transgenic mice. Synapsin I staining of 20-μm-thick cortical sections from (a) non-transgenic (Non-Tg) as well as TAR DNA-binding protein 43 (TDP-43) transgenic mice treated with (b) dimethyl sulfoxide (DMSO) (control), (c) nilotinib or (d) bosutinib. (e) Optic density of Synapsin I as a percentage of control levels. Western blot analysis of human neuroblastoma SH-SY5Y cell extracts on 12% NuPAGE SDS gel showing (f) TDP-43 expression (first blot) and Synapsin I (second blot) relative to actin (third blot) after 24 h transfection with TDP-43 cDNA and 12-h treatment with nilotinib or bosutinib ($n = 4$). Histograms (g) show densitometry of western blots. Real-time PCR showing (h) TDP-43 mRNA (first blot) and Synapsin I mRNA (second blot) levels relative to GAPDH (third blot) after 24 h transfection with TDP-43 cDNA and 12-h treatment with nilotinib or bosutinib ($n = 4$), and (i) shows RT-PCR quantification. Asterisk indicates significantly different from non-transgenic, mean ± SEM, ANOVA, Neumann–Keuls, $n = 3$. *$p < 0.05$, **$p < 0.01$, ***$p < 0.001$.

non-transgenic levels, TDP-43 transgenic mice have significantly lower optic density (24.75%, Fig. 3e, $n = 3$ per group). Treatment with nilotinib increases optic density to 70.25%, and this level is significantly lower than non-transgenic and significantly higher than transgenic treated with DMSO (Fig. 3e, $n = 3$). Treatment with bosutinib increases optic density to 58.66%, and this level is also significantly lower than non-transgenic and significantly higher than transgenic treated with DMSO (Fig. 3e, $n = 3$). The optic density in bosutinib-treated animals is significantly lower than animals treated with nilotinib (Fig. 3e, $n = 3$).

To test whether TDP-43 alters Synapsin I expression and delineate the effects of TKI treatment, we over-expressed human TDP-43 in neuroblastoma SH-SY5Y cells for 12 h and treated with nilotinib or bosutinib for an additional 12 h. TDP-43 expression was significantly increased compared to control (Fig. 3f and g, $n = 4$, first blot) and nilotinib and bosutinib significantly reduced TDP-43 levels. TDP-43 over-expression was associated with significant reduction of Synapsin I levels (second blot) and nilotinib and bosutinib reversed Synapsin I levels back to control. RT-PCR also shows that TDP-43 mRNA (Fig. 3h and i, $n = 4$, first blot) was significantly increased in cells transfected with TDP-43 with and without TKI treatment, indicating that nilotinib and bosutinib do not affect TDP-43 expression. However, TDP-43 expression significantly reduced Synapsin I mRNA, but TKI treatment that reduced TDP-43 protein levels led to reversal of Synapsin I mRNA, suggesting that TDP-43 may inhibit Synapsin I expression.

GFAP expression is reduced in TDP-43 transgenic mice and TKI treatment rescues astrocytes

Because NMR data suggested that transgenic TDP-43 mice have altered astrocyte function, fluorescent IHC was performed on cortical sections from non-transgenic as well as transgenic mice treated with DMSO, nilotinib or bosutinib. GFAP is an astrocyte-specific marker used for these IHC experiments. We previously demonstrated that TKI treatment does not affect the levels of microglia, astrocytes and dentritic cells in wild-type mice (Lonskaya *et al.* 2015), therefore, here we focus on TKI effects in TDP-43-expressing mice. The cortex of DMSO-treated TDP-43 mice (Fig. 4b, $n = 4$, inset is higher magnification from different slide) had increased TDP-43 expression compared to non-transgenic cortex (Fig. 4a and e, $n = 4$, inset is higher magnification from different slide) and no change in GFAP expression, which is normally undetectable in the cortex. Nilotinib reduced TDP-43 in the cortex and increased GFAP expression (Fig. 4c and e, $n = 4$, inset is higher magnification from different slide) compared to DMSO-treated mice. Similar changes were seen in mice treated with bosutinib (Fig. 4d–e, $n = 4$, inset is higher magnification from different slide). IHC of the hippocampus revealed a similar increase in TDP-43 expression, accompanied by loss of GFAP expression in TDP-43 mice (Fig. 4g and j, $n = 4$, inset is higher magnification from different slide). TKI treatment reduced TDP-43 expression and increased GFAP expression (Fig. 4h–j, $n = 4$, inset is higher magnification from different slide). These findings indicate that astrocytes are impaired in TDP-43 transgenic mice and support the findings of decreased astrocyte function shown by NMR (Fig. 1).

Next, we used the ionized calcium-binding adaptor molecule 1 (Iba-1), a microglia/macrophage-specific protein, to identify microglia. Fluorescent IHC did not reveal any differences in microglia level or activation as evidenced by Iba-1 staining between the four treatment groups (Fig. 4k–n).

TDP-43 over-expression did not affect the levels of EAAT1 (Fig. 4o, $n = 4$) or EAAT2 relative to actin, and TKI expression did not change the levels of these transporters.

TKIs restore alterations in mitochondrial TCA cycle in TDP-43 transgenic mice

Previous work demonstrated that TDP-43 expression increases cell death (Hebron *et al.* 2013; Chen *et al.* 2014) and TKIs induce autophagic TDP-43 clearance and reduce cell death (Chen *et al.* 2014). NMR spectroscopy was performed in total brain extracts to determine the effects of neuronal TDP-43 over-expression on mitochondrial tricarboxylic acid (TCA) cycle and oxidative stress. Pyruvate can be converted in cells into either acetyl-CoA, which then enters the mitochondrial TCA cycle, or into lactate in the cytosol, indicating oxidative stress. An increase in the levels of lactate also indicates that pyruvate is not entering into the TCA cycle, which is necessary for production of ATP for energy. TDP-43 over-expression significantly increased ^{13}C concentration in lactate (Lac) C3 compared to non-transgenic mice (Fig. 5a, $n = 4$). Both nilotinib and bosutinib decreased concentrations of ^{13}C-labeled Lac C3 (Fig. 5a, $n = 4$). ^{1}H MRS showed that TDP-43 transgenic mice have a significantly higher level of total lactate compared to non-transgenic mice, and this increase is reversed by treatment with nilotinib and bosutinib (Fig. 5b, $n = 4$). Succinate and citrate are two intermediates of the TCA cycle. Acetyl-CoA is converted into citrate by citrate synthase, and succinate is a downstream intermediate produced by conversion of succinyl-CoA by succinyl-CoA synthetase. ^{13}C MRS showed that TDP-43 transgenic mice have significantly lower ^{13}C concentration in both Succ C2/C3 and citrate C2 compared to non-transgenic mice (Fig. 5c, $n = 4$). Treatment with nilotinib restores these concentrations to non-transgenic levels (Fig. 5c, $n = 4$), but bosutinib does not change these concentrations, and these mice have significantly lower ^{13}C concentration in both Succ C2/C3 and citrate C2 (Fig. 5c, $n = 4$). ^{1}H MRS showed total levels of succinate and citrate are significantly lower in TDP-43 transgenic mice than non-transgenic mice (Fig. 5d, $n = 4$). Nilotinib restores succinate and citrate pools to non-transgenic levels (Fig. 5d, $n = 4$).

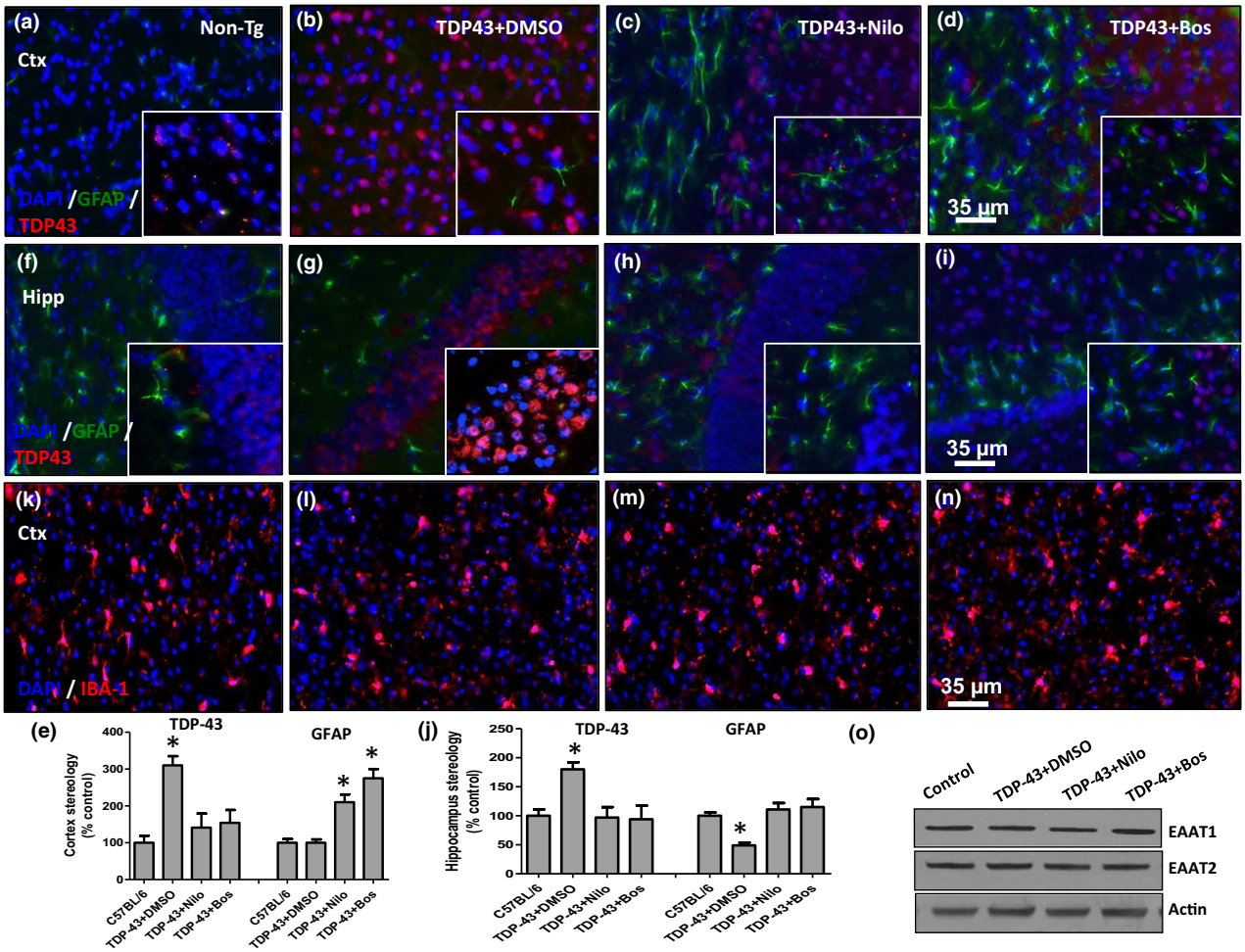

Fig. 4 Immunofluorescence of mouse cortex and hippocampus shows changes in astrocyte expression in transgenic mice. Immunofluorescence of 20-µm-thick brain sections for: glial fibrillary acidic protein (GFAP), TAR DNA-binding protein 43 (TDP-43) and DAPI in the cortex of (a) non-transgenic mice, inset is higher magnification from different slide (b) TDP-43 transgenic mice treated with dimethyl sulfoxide (DMSO) (control). Inset is higher magnification from different slide. (c) TDP-43 mice treated with nilotinib and (d) bosutinib. Inset is higher magnification from different slide. (e) Stereological data of number of TDP-43- and GFAP-positive cells in the cortex as a percent of control. Immunofluorescence of GFAP, TDP-43 and DAPI in the hippocampus of (f) non-transgenic mice, (g) TDP-43 transgenic mice treated with DMSO, (h) TDP-43 mice treated with nilotinib and (i) bosutinib. Insets are higher magnification from different slides. (j) Stereological data of number of TDP-43- and GFAP-positive cells in the hippocampus as a percent of control. Immunofluorescence of Iba-1 and DAPI in the cortex of (k) non-transgenic mice, (l) TDP-43 transgenic mice treated with DMSO, (m) TDP-43 mice treated with nilotinib and (n) bosutinib. Western blot analysis of human whole brain extracts on 12% NuPAGE SDS gel showing (o) excitatory amino acid transporters (EAAT)1 (first blot) and EAAT2 (second blot) levels relative to actin (third blot) in mice treated with nilotinib or bosutinib ($n = 4$). $N = 4$. Asterisk indicates significantly different from non-transgenic, mean ± SEM, ANOVA, Neumann–Keuls, $n = 4$. *$p < 0.05$.

Bosutinib does not alter these levels, and the succinate and citrate pools are significantly lower in bosutinib-treated mice than non-transgenic mice (Fig. 5d, $n = 4$).

TDP-43 over-expression and the effects of TKI on the brain immune profile in TDP-43 mice

In order to determine the source of synaptic and neurotransmitter changes in the brain, we measured inflammatory markers in brain lysates of non-transgenic and TDP-43 transgenic mice treated with DMSO, nilotinib or bosutinib using Milliplex ELISA. This highly sensitive and unbiased assay allows for precise measurements of several different analytes in a sample. Nilotinib and bosutinib do not change the brain or blood inflammatory profile in wild-type mice as we demonstrated previously (Lonskaya *et al.* 2015). In comparing TDP-43 mice treated with either nilotinib or bosutinib to TDP-43 mice treated with DMSO, TKI treatment did not cause any changes in the pro-inflammatory cytokines interleukin (IL)-1α, IL-1β, IL-6 or tumor necrosis factor-α; the anti-inflammatory markers IL-4, IL-10 or IL-13;

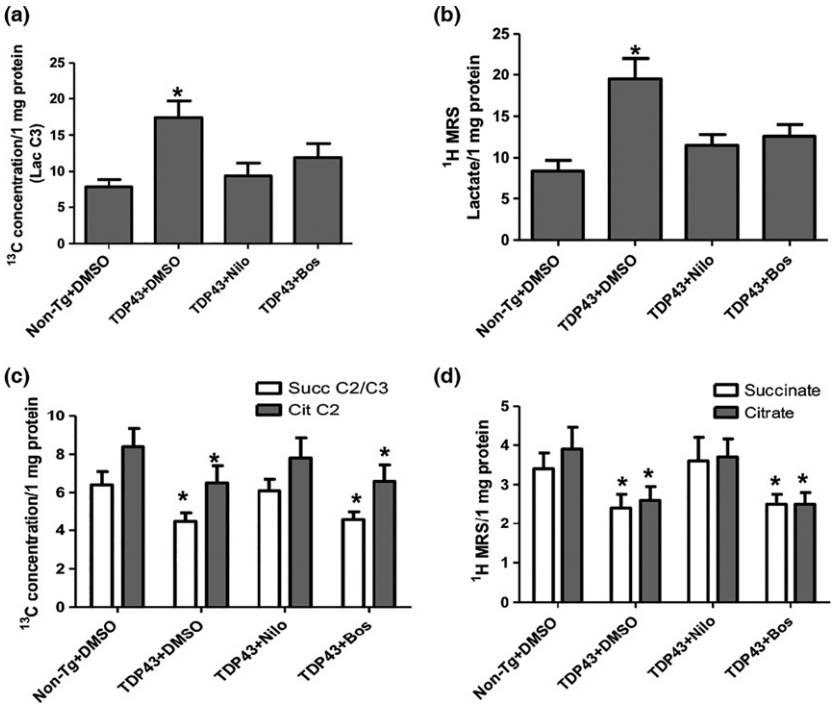

Fig. 5 High-frequency ^{13}C nuclear magnetic resonance spectroscopy reveals alteration in the levels of tricarboxylic acid cycle intermediates. Histograms represent (a) ^{13}C concentration derived from lactate C3 and (b) pool size of total lactate in hemisphere of non-transgenic as well as transgenic mice treated with dimethyl sulfoxide (DMSO) (control), nilotinib or bosutinib. (c) ^{13}C concentration in Succ C2/C3 and citrate C2 and (d) pool size of succinate and citrate in hemisphere of non-transgenic as well as transgenic mice treated with DMSO, nilotinib or bosutinib. Asterisk indicates significantly different from non-transgenic, mean ± SEM, ANOVA, Neumann–Keuls, $n = 4$. *$p < 0.05$.

the chemokines (motif) ligand (CCL)-2 and CCL-5; nor the neuromodulatory IL-2 and interferon (IFN)-γ (Table 1, $n = 4$ per treatment group). There was a significant reduction in levels of VEGF in animals treated with bosutinib compared to DMSO-treated transgenic mice (Table 1, $n = 4$ per group). Nilotinib also decreased VEGF levels, but not significantly. When comparing the TKI-treated animals to non-transgenic littermates, there were significant reductions in the level of VEGF for both nilotinib and bosutinib.

TDP-43 over-expression and TKI effect on the systemic immune profile in TDP-43 mice

We also used a Milliplex ELISA to measure inflammatory markers in the blood of these mice in order to determine whether systemic inflammatory changes reflect changes seen in the brain. In comparing TDP-43 mice treated with either nilotinib or bosutinib to TDP-43 mice treated with DMSO, TKI treatment did not cause any changes in the pro-inflammatory cytokines interleukin (IL)-1α, IL-1β or tumor necrosis factor-α; the anti-inflammatory markers IL-4, IL-10 or IL-13; the chemokines (motif) ligand (CCL)-2 and CCL-5; the neuromodulatory IL-2 and interferon (IFN)-γ; nor the growth factor VEGF (Table 2, $n = 4$ per treatment group). There was a significant increase in the level of IL-6 in the blood of transgenic mice treated with bosutinib compared to those treated with DMSO (Table 2, $n = 4$ per group). This increase was even more pronounced when comparing to IL-6 levels in the blood of non-transgenic littermates (Table 2, $n = 4$ per group).

Discussion

Our data show that the homozygous TDP-43 transgenic mice develop very early weakness, paralysis, hunch back and die pre-maturely. Homozygous mice display ALS-like symptoms, but they are difficult to work with because of their short life span. On the other hand, hemizygous TDP-43 mice do not exhibit the muscle weakness and symptoms seen in homozygous over-expressers, but they are hyperactive and spend less time in the center zone of the open field test, indicating anxiety. Furthermore, we previously demonstrated that hemizygous TDP-43 mice develop both motor and cognitive deficits and TKIs reverse these effects (Chen *et al.* 2014). Collectively, these data suggest that homozygous TDP-43 mice may mimic ALS pathology, including weakness, paralysis and hunch back, but hemizygous littermates are more likely to display symptoms that are reminiscent of the motor neuron disease–FTLD–TDP phenotype, including anxiety, motor and cognitive deficits and TKIs improve these symptoms. Therefore, hemizygous TDP-43 mice can be used as a model of TDP-43 pathology in human neurodegenerative diseases.

This work shows a novel effect of neuronal TDP-43 accumulation on synaptic proteins and astrocytic function, thereby altering detoxification of presynaptic glutamate. The data show that TDP-43 expression decreases the mRNA and protein levels of Synapsin I. The effects of TDP-43 on synaptic proteins like Synapsin I and synaptotagmin may affect the release of presynaptic glutamate into the synaptic cleft, leading to glutamate accumulation and reduced

Table 1 Brain lysate multiplex analysis of 6-month-old mice shows alterations in the brain immune profile

	IL1α	IL-1β	TNFα	IL-6	IL-4	IL-10	IL-13	CCL-2	CCL-5	IL-2	IFNγ	VEGF
Non-transgenic	11.79 ± 0.65	1.7 ± 0.17	1.74 ± 0.35	4.32 ± 0.43	7.93 ± 1.75	4.17 ± 0.58	13.53 ± 1.42	5.37 ± 1.36	11.13 ± 1.65	8.94 ± 1.01	3.81 ± 0.25	6.65 ± 0.96
TDP-43 + DMSO	9.03 ± 0.88	1.28 ± 0.18	1.32 ± 0.32	4.59 ± 0.29	4.01 ± 0.49*	3.15 ± 0.23	9.92 ± 0.72	4.17 ± 0.55	5.55 ± 0.89	5.61 ± 1.03	2.89 ± 0.35	5.83 ± 0.72
TDP-43 + Nilotinib	8.14 ± 0.10	1.11 ± 0.11	1.28 ± 0.19	4.51 ± 0.58	2.59 ± 0.42	3.64 ± 0.29	12.39 ± 1.84	4.29 ± 0.44	5.12 ± 0.49	5.14 ± 0.57	3.78 ± 0.12	4.07 ± 0.48
TDP-43 + Bosutinib	5.15 ± 1.81	0.81 ± 0.16	0.94 ± 0.14	2.98 ± 0.37	2.54 ± 0.92	2.98 ± 0.52	6.77 ± 1.32	2.09 ± 0.25	4.23 ± 0.86	4.64 ± 0.25	2.99 ± 0.67	2.41 ± 0.25*

DMSO, dimethyl sulfoxide; TDP-43, TAR DNA-binding protein 43; VEGF, vascular endothelial growth factor.

Mean fluorescent intensity values, normalized to protein assay, for various immune markers in the brains of non-transgenic as well as TDP-43 transgenic mice treated with DMSO, nilotinib or bosutinib. Values shown as mean ± SEM, one-way ANOVA, Neumann–Keuls, $n = 4$ per treatment group. Asterisks indicate significant differences from TDP-43 mice treated with DMSO (*$p < 0.05$).

Table 2 Total blood multiplex analysis of 6-month-old mice shows alterations in the systemic immune profile

	IL1α	IL-1β	TNFα	IL-6	IL-10	CCL-2	CCL-5	IL-2	IFNγ	VEGF
Non-transgenic	1362.43 ± 305.86	1.97 ± 0.90	1.38 ± 0.77	16.88 ± 2.60	4.34 ± 1.31	12.5 ± 2.18	35.06 ± 11.62	6.81 ± 1.84	1.56 ± 1.33	15.44 ± 1.85
TDP-43 + DMSO	300.88 ± 121.32	1.88 ± 0.70	0.56 ± 0.27	60.81 ± 20.96	1.31 ± 0.50	15.36 ± 13.45	59.86 ± 14.23	4.50 ± 1.38	6.78 ± 4.38	14.63 ± 8.89
TDP-43 + Nilotinib	368.36 ± 201.19	6.5 ± 2.04	3.19 ± 1.46	172.29 ± 60.44	5.72 ± 1.64	21.69 ± 10.71	49.75 ± 22.07	13.50 ± 4.05	2.56 ± 0.84	15.36 ± 6.35
TDP-43 + Bosutinib	319.56 ± 103.09	1.47 ± 0.76	1.38 ± 1.05	461.56 ± 88.46***	1.69 ± 0.87	2.13 ± 0.71	55.38 ± 26.78	3.13 ± 1.41	1.16 ± 0.83	28.00 ± 17.82

DMSO, dimethyl sulfoxide; TDP-43, TAR DNA-binding protein 43; VEGF, vascular endothelial growth factor.

Mean fluorescent intensity values for various immune markers in the blood of non-transgenic as well as TDP-43 transgenic mice treated with DMSO, nilotinib or bosutinib. Values shown as mean ± SEM, one-way ANOVA, Neumann–Keuls, $n = 4$ per treatment group. Asterisks indicate significant differences from TDP-43 mice treated with DMSO (***$p < 0.001$).

conversion of glutamate to glutamine via astrocytes. These changes in synaptotagmin and Synapsin I are also consistent with alteration of glutamate metabolism and astrocytic role to detoxify glutamate, suggesting a mechanistic insight into TDP-43 function and synaptic maintenance via TDP-43 control of synaptic protein expression (Polymenidou *et al.* 2011). It is also possible that over-expression of TDP-43 in neurons can reduce the efficiency of surrounding astrocytes and impair presynaptic glutamate–glutamine cycle, leading to glutamate accumulation. Amino acid homeostasis is important for maintaining a normal cellular environment in the brain, and loss of homeostasis can lead to increased glutamate levels and excitotoxicity (Rothstein *et al.* 1992; Shaw and Ince 1997; Philips and Rothstein 2014), perhaps as a result of a decrease in the expression of excitatory amino acid transporters in synaptic terminals (Lin *et al.* 1998; Maragakis *et al.* 2004). Our data show that alteration of astrocytic activity and the increase in glutamate levels are independent of EAAT1 and EAAT2, consistent with previous findings that TDP-43 impairs glutamate metabolism and the neuronal-astrocytic glutamate–glutamine cycle without affecting glutamate transporters (Hebron *et al.* 2014). Furthermore, changes in glutamate to glutamine ratios as well as decreases in aspartate C3 levels indicate impaired astrocyte function. Increased levels of GABA in these mice also indicate that neurons are converting glutamate into GABA at a higher rate. This may be due to the lack of glutamate to glutamine conversion, leading to an increase in the amount of glutamate available for conversion into GABA. Glutamate conversion into GABA may be a compensatory mechanism to reduce glutamate levels in neuronal TDP-43-expressing brains.

The effects of TDP-43 on astrocytic function and metabolic activity were reversed by treatment with nilotinib and bosutinib, which do not affect the mRNA but reduce the protein level of TDP-43. We previously demonstrated that TKIs reduce nuclear and soluble TDP-43 levels and abrogate TDP-43 effects on cell death and cognitive impairment in pre-symptomatic TDP-43 mice (Chen *et al.* 2014). Here, we show that TKIs reduce TDP-43 levels and improve synaptic and astrocytic functions, leading to restoration of glutamate metabolism. Additionally, increased levels of lactate and decreased levels of the TCA cycle intermediates citrate and succinate indicate oxidative metabolism. Both nilotinib and bosutinib restore levels of lactate, but only nilotinib is able to restore levels of succinate and citrate. Nilotinib (AMN107) is a multi-target molecule that preferentially inhibits Bcr-Abl with IC50 less than 30 nM in murine myeloid progenitor cells (Amagai *et al.* 2015; Medico *et al.* 2015). Bosutinib (SKI-606) is a dual Src/Abl inhibitor with IC50 of 1.2 nM and 1 nM in cell-free assays respectively (Trimmer *et al.* 2010; Gleixner *et al.* 2011; Sarkar *et al.* 2012). The lack of bosutinib effect on mitochondrial TCA cycle intermediates succinate and citrate may be due to its affinity to inhibit Src, a tyrosine kinase that is key to modulating mitochondrial functions (Hebert-Chatelain 2013). Although bosutinib fails to reduce mitochondrial and oxidative stress, it reduces TDP-43 levels and alters its localization, suggesting that TDP-43 pathology may be independent of oxidative stress and metabolic changes. Conversely, we previously demonstrated that lentiviral TDP-43 injection into rat cortex perturbs brain metabolism, but translocation of TDP-43 from nucleus to cytosol restores amino acid metabolism without reduction of TDP-43 levels (Hebron *et al.* 2014). Taken together, these data further suggest that TDP-43 level or localization affect brain metabolism.

Previous work suggests that synaptic activity increases TDP-43 level in postsynaptic dendritic spines (Wang *et al.* 2008) and TDP-43 plays a critical role in synaptic growth, formation and pruning (Godena *et al.* 2011; Lin *et al.* 2011). We do not observe any difference in dendritic spines between non-transgenic and TDP-43 over-expressing mice. However, TKI treatment led to a significant increase in dendritic spines compared to DMSO-treated mice, indicating change of TDP-43 function via re-localization (Chen *et al.* 2014), leading to improvement of synaptic function and increase in dendritic spines. TKI treatment in TDP-43 transgenic mice indicates a positive effect on brain plasticity manifest in improvement of presynaptic terminals and increased postsynaptic spine number.

An important finding from these studies is that neuronal TDP-43 affects synaptic protein expression and TKIs can reverse these effects. Previous work in our laboratory has shown these drugs to be effective in models of Alzheimer's (Lonskaya *et al.* 2013a, 2014) and Parkinson's (Hebron *et al.* 2013, 2014) diseases and this study shows that they may be effective in a model of TDP-43 pathology. The TKIs were able to decrease TDP-43 levels, restore amino acid homeostasis, restore synaptic maintenance and increase GFAP expression, thus enhancing presynaptic terminal function. Previous studies showed that lentiviral TDP-43 over-expression leads to failure of amino acid homeostasis and cell death and these effects were reversed by Parkin (Hebron *et al.* 2013, 2014). Nilotinib and bosutinib activate Parkin and produce similar effects on TDP-43-induced cell death (Hebron *et al.* 2013, 2014; Chen *et al.* 2014).

The decrease in GFAP level may indicate inactive astrocytes in untreated TDP-43 mice because of reduced levels of synaptic glutamate. This finding suggests that neuronal expression of TDP-43 can affect glial function and alter the brain inflammatory profile. Interestingly, transgenic TDP-43 mice do not significantly differ from non-transgenic mice in the levels of brain cytokines and chemokines. This, along with the lack of microglial changes, suggests that astrocytic changes in these TDP-43 mice contribute to brain synaptic, metabolic and neurotransmitter alterations, independent of microglial or inflammatory involvement. Alternatively, neuronal expression of TDP-43 may not affect

microglia activity at least in early stages of TDP-43 accumulation, but reduces the level of astrocytic production of inflammatory markers. We showed that TKIs reduce cell death in TDP-43 mice (Chen *et al.* 2014) and bosutinib treatment leads to a significant decrease in brain VEGF levels, suggesting a response to attenuation of cell death. Additionally, bosutinib increased the systemic level of pro-inflammatory IL-6 without any effects of brain IL-6, while nilotinib had no effect on either systemic or central immune markers. Taken together, these data suggest that TKIs can attenuate TDP-43 toxicity and improve synaptic and astrocytic function, independent of microglial or other inflammatory effects.

In conclusion, our data indicate an interesting mechanism of TDP-43 over-expression and its effects on metabolism and synaptic maintenance. When over-expression is limited to neurons as in this mouse model, this does not lead to classic neuroinflammation, as shown by lack of microglial changes and lack of changes in inflammatory markers. The major effect is the alteration of synaptic proteins, impairment of the presynaptic terminal and reduction in astrocytic function. Treatment with TKIs restores synaptic protein expression and the neuronal-astrocytic glutamate-glutamine cycle via reduction in TDP-43 levels. This change in synapses is not observed when non-transgenic mice are treated with TKIs, suggesting that this effect is not because of the drugs themselves, but rather due to the drugs' ability to reduce TDP-43 levels.

Acknowledgments and conflict of interest disclosure

These studies were supported by Georgetown University funding to Charbel E-H Moussa. Charbel Moussa MD, PhD, is listed as an inventor on a pending US patent application to use tyrosine kinase inhibitors as a treatment for neurodegenerative diseases.

All experiments were conducted in compliance with the ARRIVE guidelines.

Supporting information

Additional Supporting Information may be found online in the supporting information tab for this article:

Figure S1. Characterization of mouse model.

References

Algarzae N., Hebron M., Miessau M. and Moussa C. E. (2012) Parkin prevents cortical atrophy and Aβ-induced alterations of brain metabolism: ^{13}C NMR and magnetic resonance imaging studies in AD models. *Neuroscience* **225**, 22–34.

Amagai Y., Matsuda A., Jung K., Oida K., Jang H., Ishizaka S., Matsuda H. and Tanaka A. (2015) A point mutation in the extracellular domain of KIT promotes tumorigenesis of mast cells via ligand-independent auto-dimerization. *Sci. Rep.* **5**, Article number: 9775.

Chen W., Lonskaya I., Hebron M., Ibrahim Z., Olszewski R. T., Neale J. H. and Moussa C. E. (2014) Parkin-mediated reduction of nuclear and soluble TDP-43 reverses behavioral decline in symptomatic mice. *Hum. Mol. Genet.* **23**, 4960–4969.

Danbolt N. C. (2001) Glutamate Uptake. *Prog. Neurobiol.* **65**, 1–105.

Gleixner K. V., Mayerhofer M., Cerny-Reiterer S. *et al.* (2011) KIT-D816V-independent oncogenic signaling in neoplastic cells in systemic mastocytosis: role of Lyn and Btk activation and disruption by dasatinib and bosutinib. *Blood* **118**, 1885–1898.

Godena V. K., Romano G., Romano M., Appocher C., Klima R., Buratti E., Baralle F. E. and Feiguin F. (2011) TDP-43 regulates Drosophila neuromuscular junctions growth by modulating Futsch/MAP1B levels and synaptic microtubules organization. *PLoS ONE* **6**, e17808.

Hebert-Chatelain E. (2013) Src kinases are important regulators of mitochondrial functions. *Int. J. Biochem. Cell Biol.* **45**, 90–98.

Hebron M., Lonskaya I. and Moussa C. E. (2013) Nilotinib reverses loss of dopamine neurons and improves motor behavior via autophagic degradation of α-synuclein in Parkinson's disease models. *Hum. Mol. Genet.* **22**, 3315–3328.

Hebron M., Chen W., Miessau M. J., Lonskaya I. and Moussa C. E. (2014) Parkin reverses TDP-43-induced cell death and failure of amino acid homeostasis. *J. Neurochem.* **129**, 350–361.

Hebron M., Lonskaya I., Olopade P., Selby S., Pagan F. and Moussa C. E. (2014) Tyrosine kinase inhibition regulates early systemic immune changes and modulates the neuroimmune response in α-synucleinopathy. *J. Clin. Cell. Immunol.* **5**, 259.

Honda D., Ishigaki S., Iguchi Y. *et al.* (2014) The ALS/FTLD-related RNA-binding proteins TDP-43 and FUS have common downstream RNA targets in cortical neurons. *FEBS Open Bio.* **4**, 1–10.

Kantarjian H. M., Giles F., Gattermann N. *et al.* (2007) Nilotinib (formerly AMN107), a highly selective BCR-ABL tyrosine kinase inhibitor, is effective in patients with Philadelphia chromosome-positive chronic myelogenous leukemia in chronic phase following imatinib resistance and intolerance. *Blood* **110**, 3540–3546.

Lin C. L., Bristol L. A., Jin L., Dykes-Hoberg M., Crawford T., Clawson L. and Rothstein J. D. (1998) Aberrant RNA processing in a neurodegenerative disease: the cause for absent EAAT2, a glutamate transporter, in amyotrophic lateral sclerosis. *Neuron* **20**, 589–602.

Lin M. J., Cheng C. W. and Shen C. K. (2011) Neuronal function and dysfunction of Drosophila dTDP. *PLoS ONE* **6**, e20371.

Lonskaya I., Hebron M., Desforges N. M., Franjie A. and Moussa C. E. (2013a) Tyrosine kinase inhibition increases functional parkin-Beclin-1 interaction and enhances amyloid clearance and cognitive performance. *EMBO Mol. Med.* **5**, 1247–1262.

Lonskaya I., Shekoyan A. R., Hebron M. L., Desforges N., Algarzae N. K. and Moussa C. E. (2013b) Diminished parkin solubility and co-localization with intraneuronal amyloid-beta are associated with autophagic defects in Alzheimer's disease. *J. Alzheimers Dis.* **33**, 231–247.

Lonskaya I., Hebron M., Desforges N. M., Schachter J. B. and Moussa C. E. (2014) Nilotinib-induced autophagic changes increase endogenous parkin level and ubiquitination, leading to amyloid clearance. *J. Mol. Med.* **92**, 373–386.

Lonskaya I., Hebron M. L., Selby S. T., Turner R. S. and Moussa C. E. (2015) Nilotinib and bosutinib modulate pre-plaque alterations of blood immune markers and neuro-inflammation in Alzheimer's disease models. *Neuroscience* **304**, 316–327.

Maragakis N. J., Dykes-Hoberg M. and Rothstein J. D. (2004) Altered expression of the glutamate transporter EAAT2b in neurological disease. *Ann. Neurol.* **55**, 469–477.

Medico E., Russo M., Picco G. *et al.* (2015) The molecular landscape of colorectal cancer cell lines unveils clinically actionable kinase targets. *Nat. Commun.* **6**, 7002.

Musumeci F., Schenone S., Brullo C. and Botta M. (2012) An update on dual Src/Abl inhibitors. *Future Med. Chem.* **4**, 799–822.

Neumann M., Sampathu D. M., Kwong L. K. *et al.* (2006) Ubiquitinated TDP-43 in frontotemporal lobar degeneration and amyotrophic lateral sclerosis. *Science* **314**, 130–133.

Pascual M. L., Luchelli L., Habif M. and Boccaccio G. L. (2012) Synaptic activity regulated mRNA-silencing foci for the fine tuning of local protein synthesis at the synapse. *Commun. Integr. Biol.* **5**, 388–392.

Philips T. and Rothstein J. D. (2014) Glial cells in amyotrophic lateral sclerosis. *Exp. Neurol.* **262**, 111–120.

Polymenidou M., Lagier-Tourenne C., Hutt K. R. *et al.* (2011) Long pre-mRNA depletion and RNA missplicing contribute to neuronal vulnerability from loss of TDP-43. *Nat. Neurosci.* **14**, 459–468.

Rebeck G. W., Hoe H. S. and Moussa C. E. (2010) Beta-amyloid1-42 gene transfer model exhibits intraneuronal amyloid, gliosis, tau phosphorylation, and neuronal loss. *J. Biol. Chem.* **285**, 7440–7446.

Rothstein J. D., Martin L. J. and Kuncl R. W. (1992) Decreased glutamate transport by the brain and spinal cord in amyotrophic lateral sclerosis. *N. Engl. J. Med.* **326**, 1464–1468.

Sarkar T. R., Sharan S., Wang J., Pawar S. A., Cantwell C. A., Johnson P. F., Morrison D. K., Wang J. M. and Sterneck E. (2012) Identification of a Src tyrosine kinase/SIAH2 E3 ubiquitin ligase pathway that regulates C/EBPdelta expression and contributes to transformation of breast tumor cells. *Mol. Cell. Biol.* **32**, 320–332.

Sephton C. F. and Yu G. (2015) The function of RNA-binding proteins at the synapse: implications for neurodegeneration. *Cell. Mol. Life Sci.* **72**, 3621–3635.

Shaw P. J. and Ince P. G. (1997) Glutamate, excitotoxicity and amyotrophic lateral sclerosis. *J. Neurol.* **244**, Suppl 2:S3-14.

Stallings N. R., Puttaparthi K., Luther C. M., Burns D. K. and Elliott J. L. (2010) Progressive motor weakness in transgenic mice expressing human TDP-43. *Neurobiol. Dis.* **40**, 404–414.

Trimmer C., Whitaker-Menezes D., Bonuccelli G. *et al.* (2010) CAV1 inhibits metastatic potential in melanomas through suppression of the integrin/Src/FAK signaling pathway. *Cancer Res.* **70**, 7489–7499.

Wang I. F., Wu L. S., Chang H. Y. and Shen C. K. (2008) TDP-43, the signature protein of FTLD-U, is a neuronal activity-responsive factor. *J. Neurochem.* **105**, 797–806.

Wegorzewska I., Bell S., Cairns N. J., Miller T. M. and Baloh R. H. (2009) TDP-43 mutant transgenic mice develop features of ALS and frontotemporal lobar degeneration. *Proc. Natl Acad. Sci. USA* **106**, 18809–18814.

Wils H., Kleinberger G., Janssens J. *et al.* (2010) TDP-43 transgenic mice develop spastic paralysis and neuronal inclusions characteristic of ALS and frontotemporal lobar degeneration. *PNAS* **107**, 3858–3863.

Winston C. N., Chellappa D., Wilkins T., Barton D. J., Washington P. M., Loane D. J., Zapple D. N. and Burns M. P. (2013) Controlled cortical impact results in an extensive loss of dendritic spines that is not mediated by injury-induced amyloid-beta accumulation. *J. Neurotrauma* **30**, 1966–1972.

Xu Y. F., Gendron T. F., Zhang Y. J. *et al.* (2010) Wild-type human TDP-43 expression causes TDP-43 phosphorylation, mitochondrial aggregation, motor deficits, and early mortality in transgenic mice. *J. Neurosci.* **30**, 10851–10859.

Zeng L.-H., Ouyang Y., Gazit V., Cirrito J. R., Jansen L. A., Ess K. C., Yamada K. A. and Wozniak D. F. (2007) Abnormal glutamate homeostasis and impaired synaptic plasticity and learning in a mouse model of tuberous sclerosis complex. *Neurobiol. Dis.* **28**, 184–196.